# A theoretical study of sonoluminescence

V. Kamath and A. Prosperetti
*Department of Mechanical Engineering, The Johns Hopkins University, Baltimore, Maryland 21218*

F. N. Egolfopoulos
*Department of Mechanical Engineering, University of Southern California, Los Angeles, California 90089*

(Received 22 August 1991; revised 16 October 1992; accepted 11 March 1993)

The production of OH radicals by dissociation of water vapor in oscillating argon bubbles is studied theoretically to examine a possible mechanism for the emission of the 310-nm line observed in sonoluminescence experiments. Accurate models are used for the calculation of the temperature field in the gas and for the description of the associated chemical kinetics. Heat transfer between the bubble and the liquid is found to play a dominant role in the process. At the low excitation amplitudes considered, the bubble radius is also an important parameter.

PACS numbers: 43.35.Ei, 43.35.Sx

## INTRODUCTION

Sonoluminescence, the weak light emission associated with acoustic cavitation activity, is an intriguing phenomenon still poorly understood. Several hypotheses have been put forward to explain its origin (for a good review see Verral and Sehgal, 1988), but essentially only one—rooted in the large temperatures and pressures reached in the bubbles during collapse—is compatible with the available experimental evidence. Indeed, it is firmly established that the luminescence is emitted during the compression phase of the sound field (Negishi, 1961; Gunther *et al.*, 1959; Kuttruff, 1962; Gaitan and Crum, 1990; Roy and Gaitan, 1991; Gaitan, 1990; Barber and Putterman, 1991; Barber *et al.*, 1992), which rules out the triboluminescence (Chambers, 1936, 1937; Flosdorf *et al.*, 1936), microdischarge (Frenkel, 1949; Sirotyuk, 1966), and mechanochemical (Weyl and Marboe, 1949; Weyl, 1951) theories. Insensitivity to the liquid electrical conductivity (Negishi, 1961; Jarman, 1960) is incompatible with the ballo-electric mechanism (Harvey, 1939), and the anionic one (Degrois and Baldo, 1974) is similarly incompatible with the observed dependence of the spectra upon the nature of the dissolved gas (Verral and Sehgal, 1988; Prudhomme and Guilmart, 1957; Gunther *et al.*, 1959; Margulis, 1969).

Motivated by the early computations of Noltingk and Neppiras (1950), Griffing and Sette (1955) were the first to propose that the large temperatures and pressures attained during the collapse of the oscillating bubbles excited chemical reactions responsible for the emission of light. In 1963 Hickling presented the first numerical calculations of a freely collapsing bubble in which the complete thermofluid dynamic behavior of the bubble's contents was obtained from a direct numerical solution of the conservation equations for mass, momentum, and energy in the gas. He demonstrated the large effect that the thermal conductivity of the gas has on the peak temperatures in the bubble and gave thus an explanation of the marked influence of this physical property on the earlier experimental results of Proudhomme and Guilmart (1957). More recent work confirms this strong dependence (Verral and Sehgal, 1988).

Very recently, Crum and Gaitan (Gaitan and Crum, 1990; Gaitan, 1990) gave a remarkable experimental demonstration (implicit perhaps in the 1970 work of Saksena and Nyborg; see also Crum and Reynolds, 1985) that sonoluminescence can be produced by a single stably oscillating air bubble. This discovery opened the way to a much more detailed experimental study of the process than had previously been possible and a series of striking new results is documented in the recent papers of Putterman and coworkers (Barber and Putterman, 1991, 1992; Barber *et al.*, 1992; Löfstedt *et al.*, 1993).

In their experimental study, Taylor and Jarman (1970) showed that, when water is saturated with a noble gas such as argon or xenon, the sonoluminescence spectrum exhibits a strong peak at approximately 310 nm. Sehgal *et al.* (1980,1988) showed this peak to be due to the radiative transition of excited hydroxyl radicals to the ground state,

$$H_2O^* \rightarrow H + OH^* \rightarrow H + OH + h\nu, \qquad (1)$$

where the excited $H_2O$ molecule is produced, e.g., by a molecular collision. The excited $H_2O$ also has a lower probability of a direct radiative decay with an emission in the range between 270 and 290 nm. Other mechanisms (reviewed in Verral and Sehgal, 1988) have been proposed to account for the weaker broadband background found experimentally. For air-saturated water the spectra look substantially different due to the combination of the OH emissions with those associated with the nitrogen radicals (Verral and Sehgal, 1988; Taylor and Jarman, 1970).

From the point of view of the underlying chemistry, the simplest sonoluminescence process is that involving noble gases, since in this case one only deals with the hydrogen–oxygen system, with the inert gas simply acting as a colliding agent to facilitate the unimolecular decomposition reaction of the water vapor. For this reason, in the present paper, we study the formation of hydroxyl radicals in stably oscillating bubbles containing noble gases, primarily argon. For this purpose, we combine an earlier model

 0001-4966/93/94(1)/248/13/$6.00  

for the calculation of the gas temperature field (Prosperetti *et al.*, 1988) with a detailed chemical kinetics description. We find that hydroxyl radicals are produced in a substantial number even at relatively low excitation amplitudes. In this range of stable cavitation the process exhibits a strong dependence on the bubble radius, water temperature, and other parameters.

While our study has been motivated by the recent observations of stably oscillating, light-emitting air bubbles previously mentioned, the difference in the gas composition prevents us from attempting a direct comparison with that work. Our results however seem to shed an interesting light on some fundamental physical aspects of the process. With air, the ratio of specific heats of the gas is smaller than with a noble gas and heating rates comparable to the ones found here would require larger driving pressure amplitudes. On the other hand, as far as the basic $H_2O$ molecular decomposition process is concerned, one would not expect major qualitative differences with our findings. As noted above, the simultaneous presence of different excited species would however strongly affect the spectrum of the emitted light.

## I. MODEL

With one exception to be mentioned below, the model used to describe the bubble motion is essentially that of Prosperetti *et al.* (1988), which is briefly reviewed here.

The bubble is assumed to oscillate spherically with a radius $R(t)$ determined by the Keller equation

$$\left(1-\frac{\dot R}{c}\right)R\ddot R+\frac{3}{2}\left(1-\frac{\dot R}{3c}\right)\dot R^2=\frac{1}{\rho_L}\left(1+\frac{\dot R}{c}+\frac{R}{c}\frac{d}{dt}\right)[p_B-p_A]. \tag{2}$$

Here time derivatives are denoted by dots, $c$ is the speed of sound in the liquid, and $\rho_L$ is the liquid density. The instantaneous ambient pressure in the liquid, including the sound field, is denoted by $p_A$. In this work we shall take

$$p_A=p_\infty(1-\epsilon\cos\omega t), \tag{3}$$

where $p_\infty$ is the undisturbed static pressure (taken as 1 bar—0.1 MPa—in the calculations that follow), $\omega$ is the angular frequency of the sound field, and $\epsilon$ its dimensionless pressure amplitude. The liquid pressure just outside the bubble surface, $p_B$, is related to the internal gas pressure $p$ by

$$p+p_v=p_B+\frac{2\sigma}{R}+4\mu\frac{\dot R}{R}, \tag{4}$$

where $p_v$ is the vapor pressure, $\sigma$ the surface tension coefficient, and $\mu$ the liquid viscosity. At 20 °C the vapor pressure of water is about 0.02 bars and therefore very small compared with the partial pressure of the gas necessary to maintain the bubble in equilibrium. As the bubble expands, this partial pressure falls while $p_v$ remains essentially constant (Plesset and Prosperetti, 1977). However, by the time $p\simeq p_v$, the pressure in the bubble is negligible anyway and the motion is governed by $p_A$ and inertial effects. When the bubble contracts, as will be seen below, its surface temperature increases somewhat and so will therefore $p_v$. The gas pressure, however, increases by orders of magnitude so that, again, $p_v$ has little impact on the dynamics. Hence, in the following, we shall disregard altogether this contribution in Eq. (4).

A major assumption that we now make is that the internal pressure only depends on time and is spatially uniform. This is justifiable at low excitation amplitudes (Prosperetti *et al.*, 1988; Prosperetti, 1991), but there is no assurance as to its applicability to the present conditions and, *a fortiori*, to the experiments of Gaitan and Crum (1990) and Barber *et al.* (1992) at higher pressure amplitudes. If shock waves form in the gas, our results will considerably underestimate the actual dissociation rates and light emission intensity. With the further assumption that the gas behaves according to the perfect gas laws, it can be shown that $p$ is determined by the equation (Prosperetti, 1991)

$$\dot p=\frac{3}{R}\left((\gamma-1)K\left.\frac{\partial T}{\partial r}\right|_R-\gamma p\dot R\right), \tag{5}$$

with the gas temperature $T$ to be obtained by solving (Prosperetti, 1991)

$$\frac{\gamma}{\gamma-1}\frac{p}{T}\left[\frac{\partial T}{\partial t}+\frac{1}{\gamma p}\left((\gamma-1)K\frac{\partial T}{\partial r}-\frac{1}{3}r\dot p\right)\frac{\partial T}{\partial r}\right]-\dot p$$
$$=\nabla\cdot(K\nabla T). \tag{6}$$

In these equations $\gamma$ is the ratio of the gas heat capacities and $K$ is the gas thermal conductivity.

In Prosperetti *et al.* (1988) and Kamath and Prosperetti (1989), the gas temperature equation was solved subject to the boundary condition of constant surface temperature, $T(r=R(t),\ t)=T_\infty$, where $T_\infty$ is the undisturbed liquid temperature. This procedure was justified with the following argument. If $T_L$ and $K_L$ denote the liquid temperature and thermal conductivity, and phase change effects are unimportant, conservation of energy at the bubble interface requires continuity of the heat flux

$$K\frac{\partial T}{\partial r}=K_L\frac{\partial T_L}{\partial r}. \tag{7}$$

The temperature gradients can be estimated by introducing thermal layer thicknesses $\delta_G$ and $\delta_L$

$$\frac{\partial T}{\partial r}\sim\frac{T_G-T_S}{\delta_G},\quad \frac{\partial T_L}{\partial r}\sim\frac{T_S-T_\infty}{\delta_L}, \tag{8}$$

where $T_G$ is the temperature of the bubble "core" and $T_S$ the surface temperature. By using the estimates $\delta\sim\sqrt{D\,\Delta t}$, where $\Delta t$ is a characteristic time (e.g., the oscillation period) common to the gas and the liquid and $D$ the thermal diffusivity, one then obtains from (7)

$$\frac{T_S-T_\infty}{T_G-T_S}=\left(\frac{KC_{pG\rho G}}{K_LC_{pL\rho}}\right)^{1/2}, \tag{9}$$

where $C_p$ is the specific heat per unit mass. The term in the right-hand side is typically of the order of $10^{-3}$ or $10^{-2}$, which shows that the majority of the temperature drop

TABLE I. The chemical kinetic model used in the calculations. The constants $k_f$ and $k_b$ are used in the calculation of the forward and backward reaction rates, respectively, according to Eqs. (15) and (17). Activation energies $E_a$, $E_b$ in calories per mole, concentrations in moles per cm$^3$. The notation used in the columns labeled $A_f$ and $A_b$ is such that, e.g., $1.92D14 = 1.92\times10^{14}$, etc.

| No. | Reaction | $A_f$ | $\beta_a$ | $E_a$ cal/mol | $A_b$ | $\beta_b$ | $E_b$ cal/mol |
|---|---|---|---|---|---|---|---|
| 1 | $H+O_2=O+OH$ | $1.92D14$ | 0.0 | 16440 | $7.18D11$ | 0.36 | −679 |
| 2 | $O+H_2=H+OH$ | $5.08D4$ | 2.67 | 6292 | $2.64D4$ | 2.65 | 4462 |
| 3 | $OH+H_2=H+H_2O$ | $2.18D8$ | 1.51 | 3430 | $1.02D9$ | 1.51 | 18620 |
| 4 | $OH+OH=H_2O+O$ | $2.1D8$ | 1.4 | 397 | $2.21D9$ | 1.4 | 16628 |
| 5 | $H_2+M=H+H+M$ Coef. $H_2$/2.5/$H_2O$/16.0/ | $4.58D19$ | −1.4 | 104400 | $2.45D20$ | −1.78 | 960 |
| 6 | $O+O+M=O_2+M$ Coef. $H_2$/2.5/$H_2O$/16.0/ | $6.17D15$ | −0.5 | 0 | $1.58D17$ | −0.5 | 118182 |
| 7 | $O+H+M=OH+M$ Coef. $H_2O$/5.0/ | $4.72D18$ | −1.0 | 0 | $4.66D17$ | −0.65 | 101660 |
| 8 | $H+OH+M=H_2O+M$ Coef. $H_2$/2.5/$H_2O$/16.0/ | $2.25D22$ | −2.0 | 0 | $1.96D22$ | −1.62 | 118600 |
| 9 | $H+O_2+M=HO_2+M$ Coef. $H_2$/2.5/$H_2O$/16.0/ | $2.00D15$ | 0 | −1000 | $2.46D15$ | 0 | 48290 |
| 10 | $HO_2+H=H_2+O_2$ | $6.63D13$ | 0 | 2126 | $2.19D13$ | 0.28 | 56420 |
| 11 | $HO_2+H=OH+OH$ | $1.69D14$ | 0 | 874 | $1.08D11$ | 0.61 | 36220 |
| 12 | $HO_2+O=OH+O_2$ | $1.81D13$ | 0 | −400 | $3.1D12$ | 0.26 | 51832 |
| 13 | $HO_2+OH=H_2O+O_2$ | $1.45D16$ | −1.0 | 0 | $2.18D16$ | −0.72 | 69181 |
| 14 | $HO_2+HO_2=H_2O_2+O_2$ | $3.0D12$ | 0 | 1387 | $4.53D14$ | −0.39 | 39140 |
| 15 | $H_2O_2+M=OH+OH+M$ Coef. $H_2$/2.5/$H_2O$/16.0/ | $1.2D17$ | 0 | 45500 | $9.D11$ | 0.90 | −6062 |
| 16 | $H_2O_2+H=H_2O+OH$ | $3.2D14$ | 0 | 8960 | $1.14D9$ | 1.36 | 75870 |
| 17 | $H_2O_2+H=H_2+HO_2$ | $4.82D13$ | 0 | 7948 | $1.41D11$ | 0.66 | 24480 |
| 18 | $H_2O_2+O=OH+HO_2$ | $9.55D6$ | 2 | 3970 | $4.62D3$ | 2.75 | 18435 |
| 19 | $H_2O_2+OH=H_2O+HO_2$ | $1.00D13$ | 0 | 1800 | $2.8D13$ | 0 | 32790 |

from $T_G$ to $T_\infty$ occurs from the bubble core to the surface and that $T_S$ cannot differ greatly from $T_\infty$. In spite of this argument, in order to avoid any ambiguity deriving from the assumption of a constant surface temperature, in this paper we shall also calculate the temperature field in the liquid. For this purpose we need to solve the equation

$$\rho L C_{pL}\left(\frac{\partial T_L}{\partial t}+\frac{R^2\dot{R}}{r^2}\frac{\partial T_L}{\partial r}\right)=\nabla\cdot(K_L\nabla T_L), \tag{10}$$

in the domain $R(t)\leqslant r\leqslant\infty$. This is the only point in which the present model differs from the earlier one of Prosperetti *et al.* (1988). Since the effect of liquid compressibility on the velocity field is very small, we have used the incompressible expression of this quantity in the convective part of the time derivative. The two temperature fields obtained from (6) and (10) must be matched at the bubble interface where the continuity of heat fluxes (7) and of temperatures

$$T(r=R(t),t)=T_L(r=R(t),t), \tag{11}$$

must be imposed. It will be seen that the results confirm the anticipated smallness of the heating of the liquid.

In the calculations we shall take all physical properties to be constant except for the gas thermal conductivity for which a linear relation

$$K(T)=A+BT, \tag{12}$$

is assumed. For argon we use $A=0.009$ W/m K, $B=3.2\times10^{-5}$ W/m K$^2$, which give a reasonable representation of measured values over the range from 250 to 2000 K which is the only one where data are available (Cook, 1961). For neon we take $A=0.0159$ W/m K, $B=10^{-4}$ W/m K$^2$ which fits the data over the interval from 90 to 1600 K.

## II. CHEMICAL KINETICS

As stated in the Introduction, there are indications that the strong 310-nm peak observed in sonoluminescence spectra is due to the radiative decay of the hydroxyl radical from an excited state. The simplest situation to study is that in which the water undergoes unimolecular decomposition upon collision with an inert gas since in this case only the hydrogen/oxygen reaction scheme is needed. Here we mainly consider argon, which is also found experimentally to give rise to the "cleanest" sonoluminescence spectrum (Verral and Sehgal, 1988; Taylor and Jarman, 1970; and Sehgal *et al.*, 1980). We also briefly consider neon to explore the effect of the gas thermal conductivity.

The kinetic scheme that we use, developed along the lines of Egolfopoulos and Law (1990), can be equally applied to both cases and is shown in Table I. It includes the elementary reactions between stable species and free radicals for the oxygen/hydrogen system that can be of relevance to the present study. Even though we are dealing with one of the simplest reacting systems, the scheme is rather complex. The study of air bubbles would increase the complexity considerably because of the need to account for the nitrogen reactions as well. That the nitrogen chemistry plays an important role is confirmed experimentally by the marked difference between the spectra found with air and inert gases.

For each species appearing in Table I, e.g., $H$, we write a rate equation of the form

$$\frac{d[H]}{dt}=\sum(\text{production})-\sum(\text{destruction}), \tag{13}$$

where $[H]$ is the concentration of atomic hydrogen and the first sum contains the contributions of all reactions producing $H$, and the second one that of all the reactions consuming $H$. For example, for the first reaction in the table, the forward process corresponds to a consumption of $H$ and thus contributes the term

$$k_f[\mathrm{H}][\mathrm{O}_2], \tag{14}$$

to the second summation in (13). Here $k_f$ is the forward reaction rate for reaction No. 1 and is parametrized in the modified Arrhenius form

$$k_f=A_f T^{\beta_a}\exp(-E_a/\mathscr{R}T), \tag{15}$$

where $\mathscr{R}$ is the universal gas constant and the constants $A_f$, $\beta_a$, and $E_a$ are given in the first line of the table. Reaction No. 1 in the backward direction, on the other hand, produces $H$, and therefore contributes to the first summation in (13) the term

$$k_b[\mathrm{O}][\mathrm{OH}], \tag{16}$$

with the backward reaction rate

$$k_b=A_b T^{\beta_b}\exp(-E_b/\mathscr{R}T). \tag{17}$$

For the three-body backward reaction No. 5 the contribution to the last term of (13) is

$$Ck_b[H]^2[M], \tag{18}$$

where $M$ stands for any third molecule. The multiplicative coefficient $C$ indicated in the second line of the table entry is 1 if $M$ is a noble gas atom, but should be taken as 2.5 for collisions involving an $H_2$ molecule and as 16 for collisions with an $H_2O$ molecule. The same convention applies to all reactions involving $M$ in the table.

The scheme of Table I has been partially validated from hydrogen flame studies (Egolfopoulos and Law, 1990) as well as shock-tube and reactor-type experiments (Yetter *et al.*, 1991). The backward rates indicated have been determined from the forward rates and thermodynamic equilibrium by using the thermodynamic data of Kee *et al.* (1987). It should be emphasized, however, that the unimolecular-decomposition reactions, as described in Table I, have been tested experimentally only up to about 30 bars. For higher pressures a gradual modification of the rates is expected according to the Lindemann mechanism (Gardiner and Troe, 1984) which is basically an asymptotic approach toward the high-pressure limit. This change, however, is not expected to affect qualitatively the physics and conclusions drawn below, since its net effect will only be to decrease somewhat the rates from the values used in the present calculation.

## III. NUMERICAL METHOD

It is convenient for numerical work to deal with a fixed rather than a moving boundary. We achieve this objective by introducing the new radial variable

$$y=r/R(t). \tag{19}$$

It is also convenient to transform the unbounded domain occupied by the liquid into a bounded one, and for this purpose we use the algebraic transformation

$$1/\xi=1+(y-1)/L, \tag{20}$$

where $L$ is chosen to be proportional to the diffusion length in the liquid,

$$L=l(D_L/\omega R_0^2)^{1/2}, \tag{21}$$

in which $D_L=K_L/C_{pL}\rho_L$ is the liquid thermal diffusivity and $l$ a numerical constant for which the value $l=20$ has been chosen for the calculations after some trials. With the mapping (20) the bubble boundary $r=R(t)$ is transformed to $\xi=1$ while infinity corresponds to $\xi=0$. Thus, with the use of Chebyshev polynomials, we gain an excellent resolution in the thermal boundary layer adjacent to the bubble.

The numerical algorithm that has been used to solve the partial differential equations (6) and (10) is based on a collocation form of the pseudospectral method which is extensively documented (Gottlieb and Orszag, 1977; Canuto *et al.*, 1988). An earlier application to a similar problem in gas bubble dynamics may be found in Kamath and Prosperetti (1989) which also contains a more detailed description of the method. The temperature fields are first approximated by their projections onto a basis of Chebyshev polynomials. In view of the conditions of zero gradient at the bubble center ($y=0$) and at infinity ($\xi=0$), only the even polynomials $T_{2k}$ are required. Thus, the temperature field in the liquid is approximated by

$$\theta\equiv\frac{T_L}{T_\infty}\simeq\theta^M=\sum_{k=0}^{M} b_k(k)T_{2k}(\xi). \tag{22}$$

The liquid energy equation (10) may be compactly written

$$\frac{\partial\theta^M}{\partial t}=\mathscr{D}[\theta^M], \tag{23}$$

where, in terms of $\xi$, the operator $\mathscr{D}$ is given by

$$\mathscr{D}=\left(\frac{\xi}{L}\right)^2\left[\frac{D_L}{R^2}\left(\xi^2\frac{\partial^2}{\partial\xi^2}+2\xi\frac{\partial}{\partial\xi}\right)\right]-\frac{\xi^2}{L}\left[\frac{2D_L}{yR^2}+\frac{\dot R}{R}\left(y-\frac{1}{y^2}\right)\right]\frac{\partial}{\partial\xi} \tag{24}$$

with $y$ given by (20) as a function of $\xi$.

By writing (23) at the Gauss–Lobatto collocation points

$$\xi_i=\cos(\pi j/2M),\quad j=0,1,\ldots,M,$$

one obtains a system of ordinary differential equations for the unknown coefficients $b_k$, $k=0,1,\ldots,M$, of the expansion (22)

$$\sum_{k=0}^{M} T_{2k}(\xi_j)\frac{db_k}{dt}=\mathscr{D}[\theta^M(\xi_j)], \tag{25}$$

for $j=1,2,...,M$; the first point $\xi_0=1$ is the bubble surface at which the boundary conditions must be applied.

A similar procedure is used for the gas temperature equation after the introduction of the auxiliary variable

$$\tau=\frac{1}{\Theta}\int_{T_\infty}^{T} K(T')dT', \tag{26}$$

where $\Theta=D(p_\infty+2\sigma/R_0)$ is a normalization constant expressed in terms of the undisturbed gas thermal diffusivity and pressure. Now the expansion analogous to (22) is

$$\tau\simeq\tau^N=\sum_{k=0}^{N} a_{2k}T_{2k}(y), \tag{27}$$

from which a form similar to (25) is obtained upon substitution into (6).

Since the previous approach reduces the problem to the solution of a system of ordinary differential equations, it is useful to recast the boundary conditions into a similar form. By differentiating with respect to time Eq. (11) we find

$$\frac{\Theta}{K(T_S)}\sum_{k=0}^{N}\frac{da_k}{dt}=T_\infty\sum_{k=0}^{M}\frac{db_k}{dt}. \tag{28}$$

Similarly, time differentiation of (7) gives

$$\Theta\sum_{k=0}^{N}(2k)^2\frac{da_k}{dt}=K_L T_\infty\sum_{k=0}^{M}(2k)^2\frac{db_k}{dt}. \tag{29}$$

The mathematical structure of the problem consists now of the $M$ differential equations (23), the analogous $N$ differential equations for the gas temperature, the boundary conditions (28), (29), the Keller equation (2), the pressure equation (5), and the chemical kinetics equations (13) written for each species appearing in Table I. Their numerical solution is effected by using Gear's method for stiff equations as implemented in the subroutine IVPAG of the IMSL package.

## IV. RESULTS

The model described above contains a large number of parameters and an extensive investigation of the relevant parameter space would require a major effort. Aside from its magnitude, a compelling reason not to embark in such a task is suggested by the imprecision with which the rates used in the chemical kinetics calculations are known at the elevated temperatures and pressures encountered in the calculations to be described. In this situation, it is better to focus on the generic features of the process which should be relatively robust and independent of the specific nature of the system investigated and of the uncertainties in the details of the kinetics. In this spirit, we shall therefore study in detail the specific case of argon bubbles in water at a frequency of 21 kHz, which is close to the frequency range of some recent experiments (Gaitan and Crum, 1990; Gaitan, 1990). These experiments have been conducted with air bubbles but, as explained before, a chemical kinetic model for air rather than argon would require many more reactions to account for the nitrogen chemistry. Because of the simultaneous light emission from the nitrogen radicals, the spectrum would also be different. Thermally, however, the primary difference between air and a noble gas would be caused by the much larger adiabatic index of a monomolecular gas, $\frac{5}{3}$ as compared to $\frac{7}{5}$. Because of this, the argon bubble heats up more effectively than an air one would and, therefore, one would expect radical production to occur at a somewhat lower pressure amplitude.

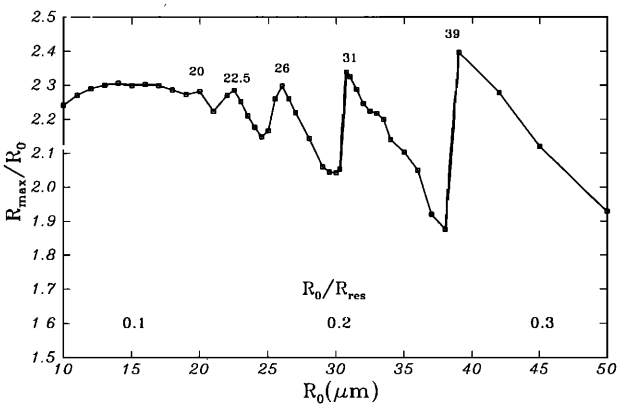


FIG. 1. Normalized maximum radius of an argon bubble during steady oscillations at 21 kHz and 0.93 relative pressure amplitude. The numbers along the curve indicate the values of the radius corresponding to the resonance peaks. The curve has been traced by linear interpolation through the computed results (squares). The radius $R_{res}$ of a bubble resonating at this frequency is 150 $\mu$m.

In a typical sonoluminescence experiment, when the sound field is turned on, no bubbles are present. Bubbles grow from a small size by rectified diffusion and coalescence with other bubbles until they become "active." The interesting region is therefore that below the resonant size, and indeed this is the region that has been investigated in the recent experiments mentioned above.

### A. Bubble dynamics

In the calculations to be described here we have used for the dimensionless forcing sound amplitude the value $\epsilon=0.93$. In this choice we have been guided by a desire to use the lowest possible level compatible with the presence of clear chemical effects. The reasons are twofold. In the first place, although state-of-the-art, the mathematical model we use is probably invalid at forcings much above 1 bar both in its chemical kinetics and bubble dynamics aspects. Second, with increasing pressure amplitudes, collapses become sharper and sharper and smaller and smaller time steps must be used with the consequence of a considerable increase in computation times. The data of Barber and Putterman (1991) and Barber *et al.* (1992) have been obtained with pressure amplitudes covering a range between somewhat less than one bar to over 5 [see Fig. 1(a) in the reference]. Crum and Gaitan's levels are between 1.1 and 1.5 bar.

We show in Fig. 1 the normalized maximum radius attained by a bubble in steady oscillations under a forcing

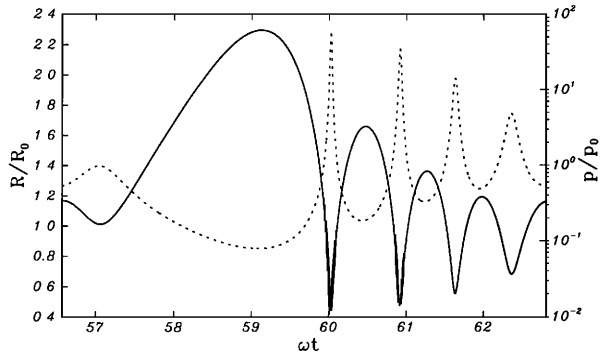


FIG. 2. Normalized radius (solid line, left scale) and internal pressure (dotted line, right scale, also shown in Fig. 3) for a 26-$\mu$m argon bubble oscillating at at 21 kHz and 0.93 relative pressure amplitude. Steady-state conditions have essentially been reached by the 10th cycle shown in the figure.

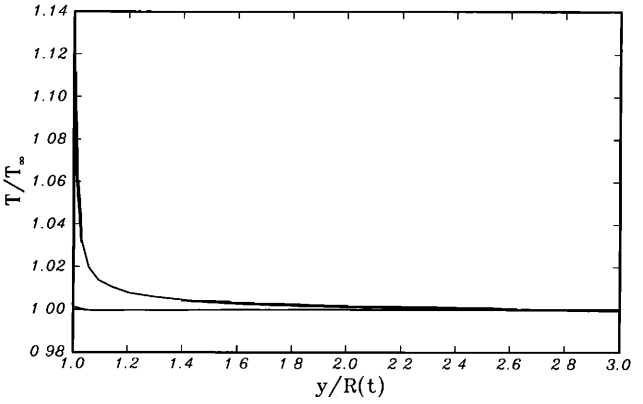


FIG. 4. Normalized temperature distribution in the liquid outside the bubble of the previous two figures at the moment of peak center temperature (upper curve) and of maximum radius (lower curve).

$\epsilon=0.93$ as a function of its equilibrium radius. The ambient pressure is 1 bar and the liquid temperature 20°. At the driving frequency of 21 kHz used in these calculations, the resonant radius $R_{res}$ is 150 $\mu$m and therefore the region comprised in the figure is for $0.067 \leqslant R_0/R_{res} \leqslant 0.33$. The peaks in the curve correspond to the nonlinear resonances occurring for $R_0=20$ $\mu$m ($R_0/R_{res}\sim 1/7$), $R_0=22.5$ $\mu$m ($R_0/R_{res}\sim 1/6$), $R_0=26$ $\mu$m ($R_0/R_{res}\sim 1/5$), $R_0=31$ $\mu$m ($R_0/R_{res}\sim 1/4$), and $R_0=39$ $\mu$m ($R_0/R_{res}\sim 1/3$).

Let us first of all consider the bubble behavior aside from sonoluminescence. In Fig. 2 we show the normalized radius (solid line, left scale) and pressure (dotted line, right scale) as a function of time for the 10th cycle of a bubble with $R_0=26$ $\mu$m, while Fig. 3 shows the pressure (dotted line, left scale) and center temperature (solid line, right scale) for the same case. The initial transient has essentially died out by this time and the conditions are very close to steady state. It is clear that the process is fairly violent with a maximum pressure of the order of 70 bar and a maximum center temperature close to 3000 K. The minimum radius reached in this case is $R_{min}=11.48$ $\mu$m and if the gas were to follow an adiabatic law, the predicted maximum temperature would be 1328 K, far less than the numerical result. The paradox can be explained by considering conduction effects in the gas. Indeed, from Fig. 3, it can be seen that the center temperature keeps rising due to conduction as the bubble hovers around its maximum radius. For this example, at the point of maximum radius, adiabatic expansion would predict a temperature of 63 K, while the model gives 275 K. Therefore, at the point where collapse begins, the temperature is not what would be predicted by the adiabatic law, but is actually close to the liquid's undisturbed temperature. A very rough approximation to this complex behavior can be obtained by assuming an isothermal expansion followed by adiabatic compression. The maximum internal temperature reached in this case is readily found to be

$$\frac{T_{max}}{T_0}=\left[\left(\frac{p_{max}}{p_{min}}\right)^{1/\gamma}\frac{p_0}{p_{min}}\right]^{\gamma-1}, \tag{30}$$

where $p_{max}$ and $p_{min}$ are the maximum and minimum values of the absolute pressure during the sound cycle. For the present driving pressure amplitude of 0.93, this expression gives $T_{max}/T_0 \simeq 22$, i.e., a center temperature well over 6000 K. These considerations clearly illustrate the great importance of heat transfer effects.

Figures 4 and 5 show the temperature distribution out-

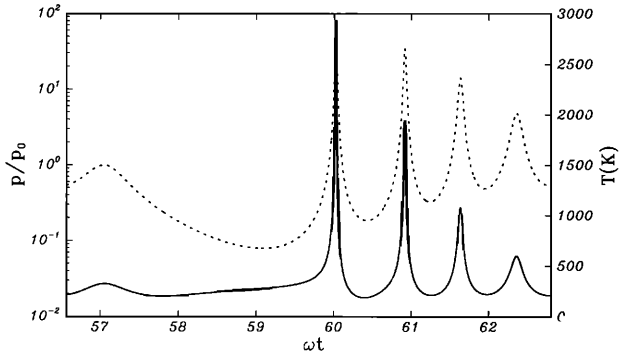


FIG. 3. Normalized internal pressure (dotted line, left scale, also shown in Fig. 2) and internal temperature at the bubble center (solid line, right scale) for a 26-$\mu$m argon bubble oscillating at 21 kHz and 0.93 relative pressure amplitude. Steady state conditions have essentially been reached by the 10th cycle shown in the figure.

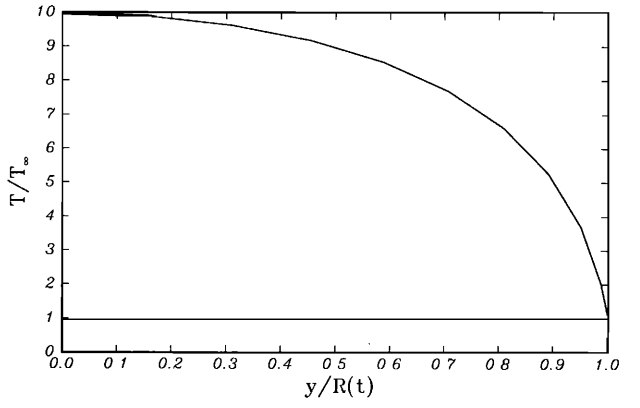


FIG. 5. Normalized temperature distribution in the gas inside the bubble of the previous three figures at the moment of peak center temperature (upper curve) and of maximum radius (lower curve).

side and inside the bubble at the instant at which the center reaches its maximum temperature (upper line) and at the instant of maximum radius (lower line). It can be seen from Fig. 4 that the temperature increase predicted to occur at the bubble wall is of the order of 40 K, so that the mean temperature gradient is about $2.5\times10^5$ K/mm! Clearly these highly unusual conditions can only be maintained due to the extremely brief persistence of the high temperature at the bubble center, which is of the order of 100 ns.

These results are typical and demonstrate the points made above on the smallness of the surface temperature rise. They however appear, at least superficially, to be in contrast with results of Suslick's (1986, 1990) who has produced convincing experimental evidence that molecular species initially in the liquid phase undergo reactions that only occur at temperatures in excess of 2000 K. Suslick (1990) suggests that these high temperatures are reached in a very thin liquid shell surrounding the bubble surface. It should be stressed that these experimental results have been obtained at pressure amplitudes of over 10 bars, far in excess of the ones used for the present calculations, so that a direct and quantitative comparison with our findings is not possible. However, it would seem that our conclusions on the modest heating of the liquid surface cast some doubt on Suslick's interpretation. A more plausible explanation may be the following. It is well known that the spherical shape of an oscillating bubble is unstable (Plesset and Prosperetti, 1977). The instability becomes particularly violent during periods of large accelerations directed into the liquid such as occur near the end of the collapse and early stages of the rebound. Pulsating bubbles have been observed to shed other small bubbles probably as a consequence of this instability (Nyborg and Hughes, 1967). The reciprocal process of tiny droplets projected into the hot bubble core can also occur, and this appears to be a more plausible mechanism by which molecules initially in the liquid phase are exposed to high temperatures. The severity of this surface disruption increases strongly with the intensity of the driving sound field. It is therefore quite possible

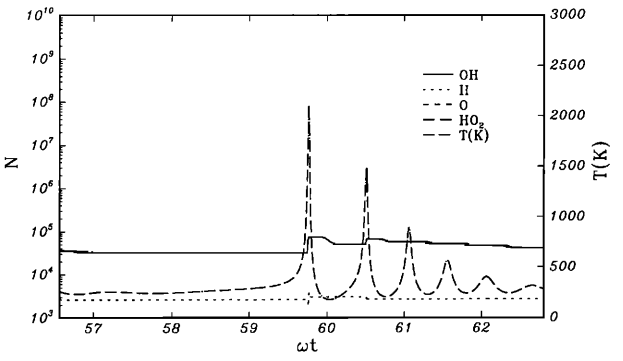


FIG. 6. Center temperature (dash-and-dots, right scale) and number of OH (solid), H (dots), O (medium dashes), and $HO_2$ (long dashes) for a 20-$\mu$m bubble at 21 kHz and 0.93 relative pressure amplitude. These numbers are obtained by multiplying the concentration evaluated in correspondence of the center temperature by the instantaneous volume of the bubble and therefore may be in error by one or two orders of magnitude. See text.

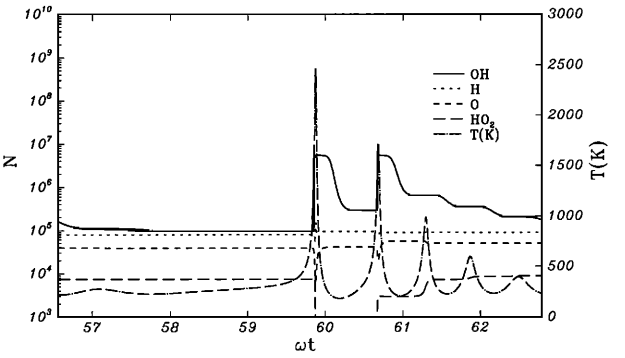


FIG. 7. Center temperature (dash-and-dots, right scale) and radical number during the 10th oscillation cycle of a 22.5-$\mu$m bubble. This value of the radius corresponds to a peak in the response curve of Fig. 1.

that extremely violent shape distortions take place at the pressure levels used by Suslick while only mild ones occur at the lower intensities used by Gaitan, Putterman, and co-workers. From the experimental evidence of stably oscillating bubbles presented by these authors, one deduces that, in a parameter range similar to the one we consider, any nonspherical effect, if present, is not strong enough to cause bubble break-up or "dancing." Hence, in spite of being based on the assumption of spherical oscillations, our model may be a reasonable approximation to the real physical situation.

According to the excited OH hypothesis, the sonoluminescence effect depends on the total number of hydroxyl radicals produced in the bubble. As the gas temperature is not uniform, in principle it would be necessary to calculate the OH concentration at a number of radial locations and determine this number by integrating the results of such calculations over the radius. For simplicity, we have not done this but we have only considered the temperature history at the bubble's center. In this way, strictly speaking, we can only calculate the concentrations in a small fraction of the bubble volume near the center. If we were to present our results by plotting these values versus time, we would not only be seeing the effect of the chemical kinetics but also those of the bubble expansion and contraction which do not have a direct bearing on the total number of molecules and radicals actually present. Therefore, we

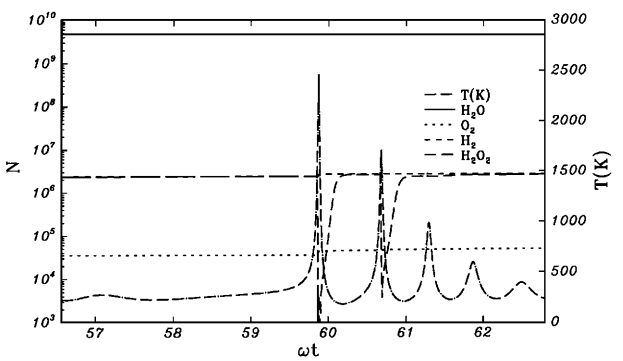


FIG. 8. Center temperature (dash-and-dots, right scale) and radical number during the 10th oscillation cycle of a 22.5-$\mu$m bubble. This value of the radius corresponds to a peak in the response curve of Fig. 1.

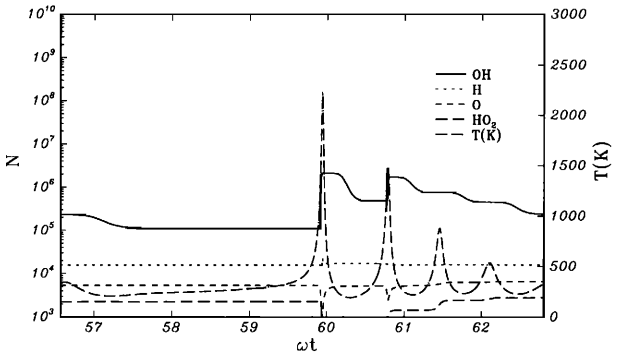


FIG. 9. Center temperature (dash-and-dots, right scale) and radical number during the 10th oscillation cycle of a 25-$\mu$m bubble. This value of the radius corresponds to a relative minimum in the response curve of Fig. 1.

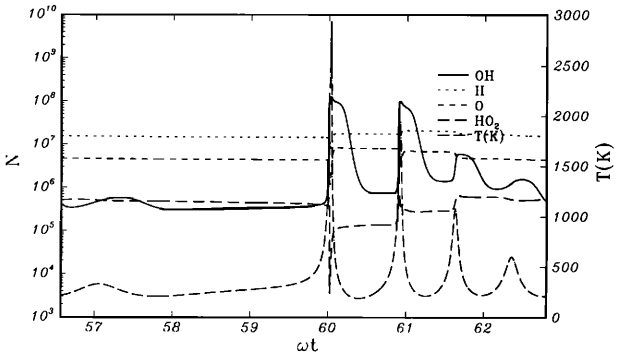


FIG. 11. Center temperature (dash-and-dots, right scale) and radical numbers during the 10th oscillation cycle of a 26-$\mu$m bubble. This value of the radius correspond to a peak in the response curve of Fig. 1.

have decided to show the computed concentrations multiplied by the instantaneous bubble volume. In this way it is easier to get a feeling for the *absolute* numbers of radicals and molecules which are the quantities of interest, although the levels indicated will represent overestimates of the actual numbers. On the basis of Fig. 5, the central region of the bubble where the temperature is relatively uniform can be estimated to extend to about 25%–50% of the radius, which corresponds to about 0.01 to 0.1 of the volume. A more realistic estimate of the actual molecular numbers would therefore be obtained by subtracting one or two orders of magnitude from the scales used in the figures below.

### B. Argon bubbles

As the discussion that follows will show, the gas temperature is the dominant variable in the production of OH radicals. Our results show that this quantity is not necessarily correlated with the maximum radius reached during the oscillations. Indeed, for example, the maximum temperature reached for the case $R_0=25$ $\mu$m (the second minimum in Fig. 1) is close to 2300 K, while for 15 $\mu$m, for which the maximum radius is larger, the maximum temperature is only 1450 K. Evidently, since conduction effects are important, the time scale over which expansion and compression occur is crucial, and this time scale is determined by the radial dynamics. At a frequency far below the resonance frequency of the bubble, compression and expansion follow the driving pressure and the bubble is essentially isothermal. As dynamical effects become more important, the bubble spends more and more time in the expanded state and collapses are shorter and shorter. The hypotheses of the crude model (30) are therefore increasingly applicable and the maximum temperature must increase. This simple argument shows that, over the span of a few $\mu$m in the value of the equilibrium radius, a threshold for radical production must be reached.

We can follow the consequences of this gradual increase in the importance of inertial effects on sonoluminescence in Figs. 6–12. Figures 6, 7, 9, and 11 show the center temperature (dash-and-dotted lines) and the corresponding radical numbers for bubble radii of 20, 22.5, 25, and 26 $\mu$m. Figures 8, 10 and 12 show the numbers of several molecular species for radii of 22.5, 25, and 26 $\mu$m. All these results are for the 10th cycle of oscillation. The solid line in Figs. 6, 7, 9, and 11 is the number of the OH radicals. A very rapid increase takes place when the temperature rises above approximately 1400 K. The temperature effect alone, however, is not sufficient to explain all the features of these curves. For instance, in Fig. 11, there is a surge of OH radicals for $\omega t \simeq 60.03$, although the center temperature is only slightly above 1000 K.

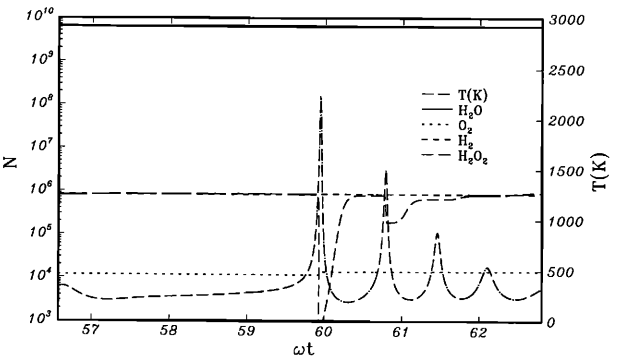


FIG. 10. Center temperature (dash-and-dots, right scale) and radical numbers during the 10th oscillation cycle of a 25-$\mu$m bubble. This value of the radius corresponds to a relative minimum in the response curve of Fig. 1.

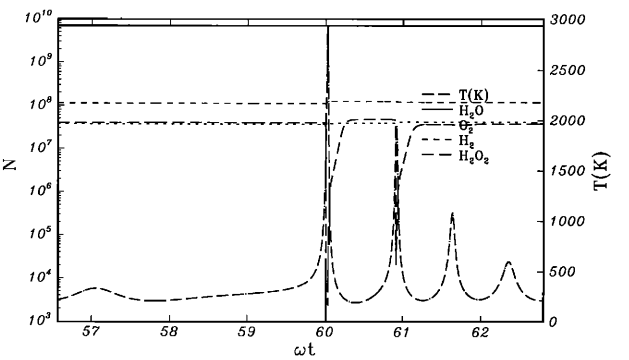


FIG. 12. Center temperature (dash-and-dots, right scale) and radical numbers during the 10th oscillation cycle of a 26-$\mu$m bubble. This value of the radius correspond to a peak in the response curve of Fig. 1.

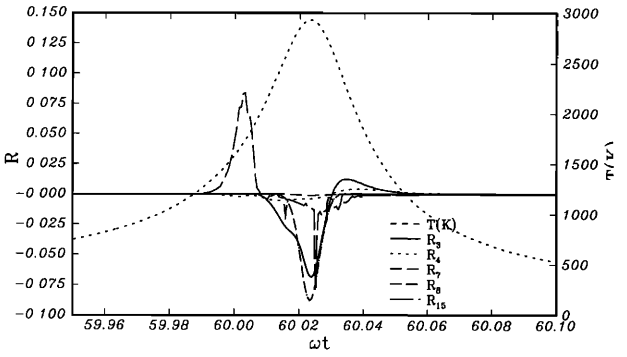


FIG. 13. Contribution of reactions Nos. 3, 4, 7, 8, 15 of Table I to the right-hand side of the OH kinetic equation around the time of peak center temperature (dotted line) for a 26-$\mu$m argon bubble.

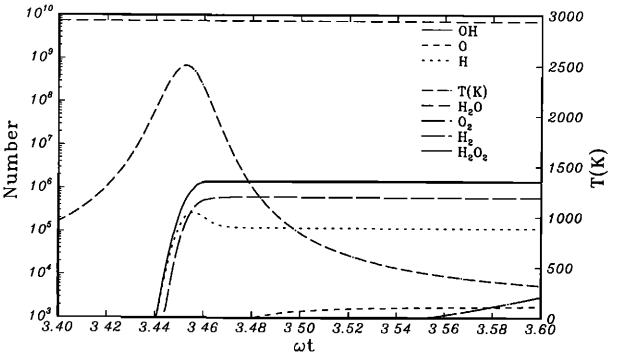


FIG. 15. Expanded detail of the previous figure near the first collapse time.

To understand this behavior it is necessary to consider in greater detail the chemical reaction rates. We plot in Fig. 13 the contribution to the right-hand side of the equation $d[\mathrm{OH}]/dt=\ldots$ given by reactions Nos. 3, 4, 7, 8, and 15 of Table I. The sign convention is such that the quantity plotted is positive if the reaction proceeds from left to right. Only a tiny and greatly enlarged fraction of the cycle around the time of maximum center temperature (dotted line) is shown here. In dimensional units the corresponding duration is about 1.14 $\mu$s. It can be seen that the earliest OH production mechanism to become important is reaction No. 15 (long dashes), i.e., the dissociation of $H_2O_2$. This molecule, once produced, remains relatively stable until it is destroyed by high-energy collisions and is therefore an important "memory mechanism" for the system. As a consequence of this dissociation, the $H_2O_2$ molecules are rapidly depleted (cf. the long-dashed line in Fig. 12). At about the point where this happens, reaction No. 3, $\mathrm{OH}+\mathrm{H}_2=\mathrm{H}+\mathrm{H}_2\mathrm{O}$ (solid line) starts producing OH, soon joined by No. 8, $\mathrm{H}+\mathrm{OH}+\mathrm{M}=\mathrm{H}_2\mathrm{O}+\mathrm{M}$ (dash-and-dot line). In order to proceed from right to left, as indicated by the negative sign of the corresponding rates, the first of these two reactions needs H radicals that Fig. 11 shows to be present in sizeable number. As a matter of fact, in all the examples shown, the number of H radicals remains essentially constant throughout the cycle and increases from about $10^3$ for $R_0=20$ $\mu$m to about $10^7$ for $R_0=26$ $\mu$m. The two other reaction rates plotted in Fig. 13, Nos. 4 (dotted line) and 7 (medium dashes), are seen to play only a minor role, and the remaining reactions of Table I are of yet smaller importance.

Another interesting aspect is the transient by which the steady state described is established. For $R_0=26$ $\mu$m we show in Fig. 14 the radical numbers during the first cycle, to be compared with Fig. 11. In Fig. 15 a magnification of the portion of the previous figure around the bubble collapse time $\omega t\simeq 3.44$ is presented, and the corresponding reaction rates are given in Fig. 16. On the basis of these results one can form the following picture of the sequence of events. As soon as the temperature and pressure become sufficiently high, water molecules start dissociating according to reaction No. 8, $\mathrm{H}+\mathrm{OH}+\mathrm{M}\leftarrow\mathrm{H}_2\mathrm{O}+\mathrm{M}$. When a sufficient amount of atomic hydrogen has formed, reaction no. 3, $\mathrm{OH}+\mathrm{H}_2\leftarrow\mathrm{H}+\mathrm{H}_2\mathrm{O}$, starts going, additional OH is formed, while H decays and $H_2$ begins to appear. The presence of a significant amount of OH also opens the way to atomic oxygen formation according to reactions Nos. 4 and 7.

Since the other reactions are found to play only a minor role in the processes described above, one may enquire whether a simplified model consisting only of reactions Nos. 3, 4, 7, and 8 would lead to similar results. We have found that the answer is in the affirmative with differences in the number of OH radicals of the order of 10% for the examples presented here. Qualitatively the major difference

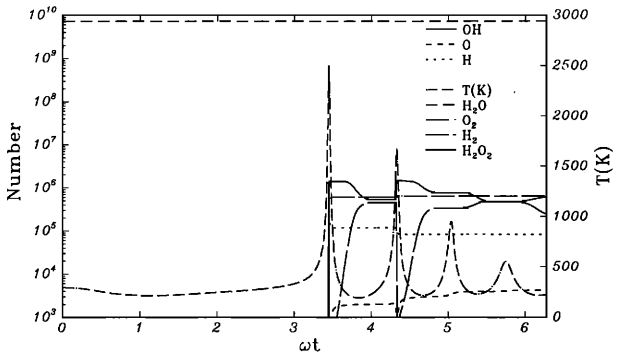


FIG. 14. Radical number during the first cycle of oscillation of a 26-$\mu$m argon bubble.

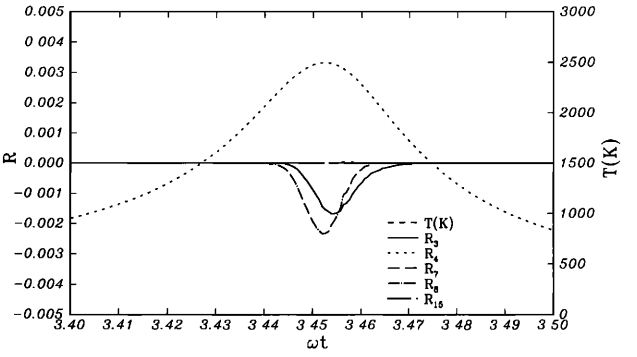


FIG. 16. Center temperature (dotted line) and contribution of reactions Nos. 3, 4, 7, 8, 15 of Table I to the right-hand side of the OH kinetic equation around the time of the first collapse (dotted line) for a 26-$\mu$m argon bubble.

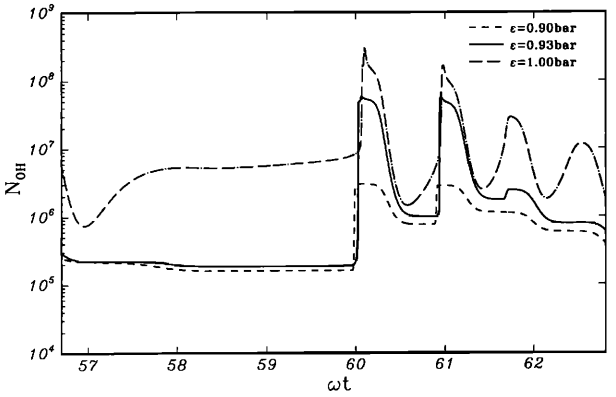


FIG. 17. Number of hydroxyl radicals during the 10th cycle of oscillation of a 26-$\mu$m bubble driven at a 0.93 relative pressure amplitude (solid), of a 26-$\mu$m bubble driven at a 1 relative pressure amplitude (dash-and-dots), and of a 27-$\mu$m bubble driven at a relative pressure amplitude of 0.9 (dashes).

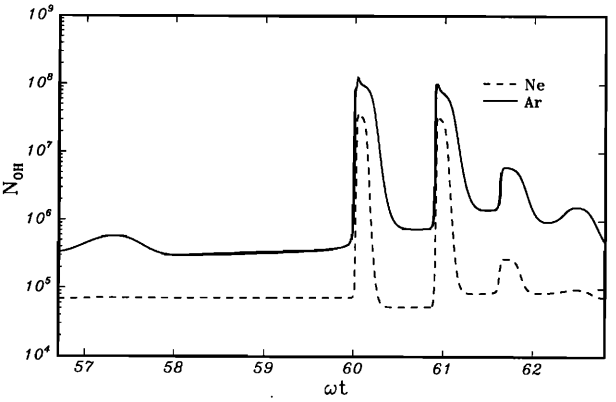


FIG. 18. Comparison of the number of hydroxyl radicals during the 10th cycle of oscillation of a 26-$\mu$m bubble containing argon (solid line) and neon (dashed line). The thermal conductivity of neon is 3–4 times that of argon.

is the absence of $HO_2$ production, which does not seem to have major consequences anyway. On the other hand, it should be stressed that this result is limited to the small parameter range that we have investigated and we do not have sufficient elements to turn it into a general conclusion.

### C. Other effects

Having looked in detail at the cases of argon bubbles, we now briefly explore the sensitivity of the results to several parameters and conditions.

In the first place, it is clear from the preceding discussion that, in the framework of the present model, the liquid temperature has a negligible effect on the radial dynamics. Since, however, the OH radicals ultimately derive from the breakup of the water vapor molecules, one should find a proportionality between the total number of hydroxyl radicals and the water vapor pressure. We have tested this prediction of the model and found it confirmed by the numerical results. For example, at 60 °C, the vapor pressure is approximately 10 times that at 20, and so is the calculated number of OH radicals. The sonoluminescent emission should exhibit a similar increase and, since the vapor pressure depends exponentially upon the liquid temperature, it should be possible to take advantage of this effect experimentally. It should be stressed that this remark is only applicable all other conditions being equal (in particular, the dissolved gas concentration and the sound pressure amplitude), which may not be easy to achieve experimentally. Of course, as the liquid temperature increases, evaporation-condensation effects at the bubble wall, neglected in the present model, become more and more important (Prosperetti *et al.*, 1988). However, for water, this should not happen below about 60 °C.

The results presented before were for a dimensionless driving pressure $\epsilon=0.93$. We compare in Fig. 17 the number of OH radicals during the tenth cycle for that case (solid line) with the number for a 26-$\mu$m bubble driven at $\epsilon=1$ (dash-and-dotted line) and a 27-$\mu$m bubble driven at $\epsilon=0.9$ (dashed line). The reason to consider a slightly bigger bubble at the lowest forcing is that, in that case, the corresponding response curve (similar to Fig. 1) is such that $R_0=26$ $\mu$m does not correspond to a peak and the OH production is therefore artificially low. Comparison of the three curves illustrates the tremendous sensitivity of the process to even small changes in the pressure amplitude, as first pointed out by Flynn (1964).

We examine the effect of the thermal conductivity of the gas by comparing in Fig. 18 the argon results (solid line) with those for neon (dashed line), both for a 26-$\mu$m bubble. The same chemical kinetic formulation can be used in both cases. The thermal conductivity of neon is about 3 to 4 times that of argon between 300 and 800 K. Correspondingly, the peak number of hydroxyl radicals is found to be about a factor of 5 smaller. In considering the implications of this comparison it should be kept in mind that, due to the difference in thermal conductivities, the internal pressure is different in the two cases.

The results of chemical kinetics calculations for the temperature histories at two other positions in the bubble, $r/R(t)\simeq 0.464$ and 0.585, corresponding to volume ratios of 10% and 20% respectively, are shown in Fig. 19. The difference between the center (solid line) and the 20%

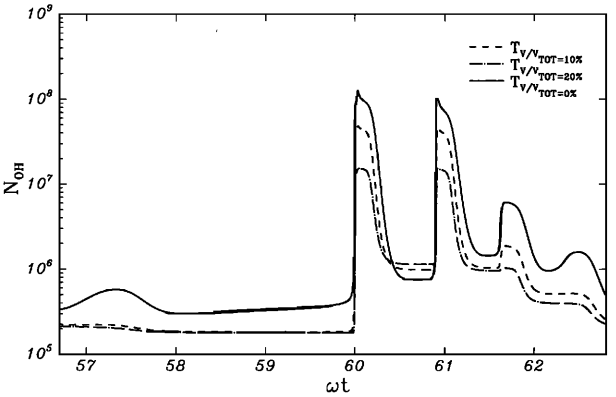


FIG. 19. Comparison between the number of hydroxyl radicals produced at different locations inside a 26-$\mu$m argon bubble driven at a relative pressure of 0.93.

result (dash-and-dotted line) is quite considerable as had been anticipated.

Finally, it may be noted that examples of chaotic radial oscillations have been reported in the literature at pressure amplitudes of the same order as the one used here (Parliz *et al.*, 1990). As shown in Kamath and Prosperetti (1989), these results are in reality due to the neglect of the thermal dissipation affecting the oscillations. Chaotic behavior does set in, but only at larger forcings, as is implicitly confirmed by the extreme regularity observed in the recent experiments. In any event, our study suggests that a sonoluminescent pulse is emitted whenever a sufficiently large compression and heating of the bubble contents takes place. At low forcing, this would occur with the same periodicity as the sound field. At higher forcing (provided of course that the bubble can still be made to levitate stably), one might expect to find the same subharmonic modulations of the light emission that are known to occur with the radius-time response and, ultimately, a chaotic behavior.

### D. Observability of sonoluminescence

In practice, observability of stable sonoluminescence emission by a single bubble requires a delicate balance. First of all, the sound amplitude and the gas concentration in the liquid must be such that the bubble stabilizes with respect to rectified diffusion. Such a stability point must occur for a value of the radius such that the rectified diffusion threshold crosses the descending portion of one of the resonance peaks shown in Fig. 1. It is only in these conditions that the equilibrium can be stable. If the bubble radius increases slightly, the oscillation amplitude decreases (see Fig. 1) and rectified diffusion is insufficient to prevent gas loss from the bubble. The radius therefore decreases, and tends to return to the previous value. The converse process occurs if the bubble radius were to decrease slightly.

A second requirement for the observability of the effect is that the sound intensity be sufficient to trap the bubble under the action of acoustic-radiation forces. Third, conditions must be such that a sufficient temperature is reached inside the bubble upon compression. In view of these requirements, observation of stable sonoluminescence should be easier with a moderately degassed liquid. Indeed, the lower the gas concentration, the higher the rectified diffusion threshold, so that equilibrium against diffusion can be achieved at acoustic pressures sufficiently large to trap the bubble and induce strong collapses. On the other hand, a lower limit to the gas concentration in the liquid would in practice be set by the onset of shape instability and erratic motion of the bubble both of which become stronger with increasing pressure amplitudes (see, e.g., Eller and Crum, 1970; Prosperetti, 1984; Horsburgh, 1991; Benjamin and Ellis, 1990). At a given frequency, one would therefore expect an optimal "window" of gas concentration.

A further parameter to which the occurrence of stable sonoluminescence should be sensitive is the liquid temperature. As noted before, all other things being equal, in a warmer liquid the concentration of vapor molecules is higher, and so will be that of OH radicals that ultimately derive from the collisional dissociation of the vapor molecules.

On the basis of our numerical results the maximum number of OH radicals reaches every cycle the order of $10^7$–$10^8$. In order to account for the temperature effect across the bubble, one or two orders of magnitude should be subtracted from these numbers as mentioned above (see Fig. 19). It is rather remarkable that a recent experiment on sonoluminescence (with air, rather than argon, bubbles, but in the same range of frequencies and pressure amplitudes) estimates that about $10^6$ photons are emitted per pulse (Barber and Putterman, 1991). Of course, our calculation gives the number of radicals instantaneously present in the bubble, which does not necessarily coincide with the number of hydroxyl-radical producing events. An estimate of this latter quantity may be obtained by comparing the time scale for production with the time during which the gas temperature remains elevated. If the former were found to be much shorter than the latter, one would conclude that many "generations" of radicals are produced (and recombine) during a single collapse event. An estimate of the hydroxyl production time scale $\tau_p$ may be obtained from

$$\tau_p = \frac{[\mathrm{OH}]}{\Sigma \text{production}}, \tag{31}$$

where $\Sigma$ production stands for the all the OH-producing terms appearing in the right-hand side of the OH rate equation. It is found that the production time scale is of the order of 1% of the sound period, and is therefore comparable with the duration of the elevated gas temperatures. This suggests that at most a few "generations" of hydroxyl radicals are produced per collapse event so that the computed number of radicals instantaneously present in the bubble coincides in order of magnitude with the number of hydroxyl-producing molecular processes actually taking place.

On the basis of these considerations one can perhaps account for the observability of stable sonoluminescence with the naked eye. A reasonable number for the minimum photon count necessary to form a perceivable image is around 100. At a distance of about 20 cm the solid angle subtended by the eye is of the order of $10^{-4}$ to $10^{-3}$ rad, so that the bubble should emit a total of $10^5$ to $10^6$ photons to be observable. This coincides with our numerical results and indicates that the effect should be directly visible in the parameter range that we have studied.

The previous considerations depict a plausible scenario and are in qualitative agreement with observation. However, it should not be forgotten that, for an OH radical to give rise to a photon, it must first be excited to a state above the ground level, a situation that we have implicitly assumed to occur with high probability. Unfortunately, we are unable to assess whether this is a reasonable assumption.

One may also speculate about sonoluminescence in a cavitating field, rather than for a single stable bubble. If the sound intensity is very strong (say, peak pressure ampli-

tudes above 4 bars or higher, depending on the frequency) the cavitation is vaporous and the lifetime of each bubble extends to one or at most very few cycles so that probably only a small number of flashes are emitted by each bubble before it shatters. At lower sound amplitudes, however, rectified diffusion plays a very important role. Nuclei start growing by this process but, as long as their radius is much smaller than the resonance radius, they pulsate following the sound pressure with negligible dynamical effects. This situation corresponds essentially to the left-hand portion of the response curve of Fig. 1. As the radius increases, the series of peaks of Fig. 1 is described in ascending order until, at some point, the collapses become strong enough to cause photonic emissions. With further growth the bubble response decreases beyond the resonance peak to increase again when the next one is encountered. [At the lower sound intensities some bubbles may be "trapped" as described above for the single-bubble case, but this should become more and more unlikely as the pressure amplitude increases as the bubbles would be much above the rectified diffusion threshold.] At some point a resonance is encountered for which the oscillation amplitude is too large for the bubble to maintain its integrity. The bubble therefore shatters producing microbubbles, which follow a similar history, possibly with the added complication of Bjerknes-force-induced coalescence. At these lower amplitudes, the bubble population is in a state of relatively slow continuous evolution, with each bubble probably emitting for many cycles during several stages of its life.

These considerations indicate that sonoluminescence emissions from stable single bubbles and from bubble fields may appear to behave quite differently experimentally. For example, it is found that bubble-field sonoluminescence intensity decreases with increasing temperature (Verral and Sehgal, 1988). This result does not necessarily falsify our opposite prediction for the single-bubble case as nucleation, and especially rectified diffusion—which is so important in the dynamics of bubble fields that it would be hard to overestimate its significance—would also be strongly affected by temperature changes.

## V. SUMMARY AND CONCLUSIONS

In earlier studies of sonoluminescence, the temperature of the gas in the bubbles has always been estimated rather crudely and it has therefore been impossible to obtain reliable reaction rates. Here we have used instead accurate models for the calculation both of the temperature field and of the associated chemical kinetics. In this way we have obtained reliable estimates of the production rates of hydroxyl radicals which are thought to be responsible for at least part of the light emitted by oscillating bubbles.

Heat transfer inside the bubble and across its interface has been found to play a very important role in the process. In particular—and contrary to statements frequently encountered in the literature—an estimate of the collapse temperature based on the adiabatic law may substantially *underpredict* the peak gas temperature because it ignores the heating of the gas by conduction while the bubble is in the expanded state. Calculations for neon, with a thermal conductivity 3–4 times larger than argon, indicate a reduced OH formation.

We have also calculated the temperature of the bubble surface and found that it changes at most by a few tens of K from the undisturbed liquid temperature. This finding seems to be in conflict with the reported fact that compounds present in the liquid, but not in the gas, phase are exposed to very large temperatures (Suslick 1990). We have proposed a mechanism to resolve the apparent paradox.

As can be seen, e.g., from Fig. 13, the persistence of a high temperature near the bubble center extends for slightly less than 1% of the cycle, or approximately 300 ns. On these grounds it is therefore impossible to account for the exceedingly short duration (currently estimated at 50 ps) of the sonoluminescence flash (Barber and Putterman, 1991; Barber *et al.*, 1992). Recent work (Greenspan and Nadim, 1993; Barber and Putterman, 1993; Löfstedt *et al.*, 1993) suggests the formation of shock waves in the gas during the compression cycle. A shock with a speed of $10^4$ m/s would traverse 1 $\mu$m in 100 ps. Such a strong shock could conceivably cause luminescence and ionization of the gas molecules. In this case, the model described in the present paper would very severely underestimate radical formation.

Another possibility might be the following. The center of the bubble is the position where radicals are first produced. Shortly thereafter, however, additional radicals are generated in the adjacent layers which could resonantly absorb and scatter the radiation coming from the center thus shutting off the observed light. The effectiveness of resonant scattering in rendering gases effectively opaque is well known since the classic 1904 experiments of Wood. This mechanism might be made more plausible by observing that, due to the condition $\partial T/\partial r=0$, the bubble core has a relatively homogeneous temperature. However, in the adjacent layers, a temperature gradient prevails and the coldest radicals would probably tend to be produced in the ground rather than in an excited state.

The time scale for this mechanism is dictated by the speed with which the temperature "wave" moves outward from the bubble center. We have calculated with our model that it takes slightly less than 1 ns for temperatures in the range 1500–2000 K to propagate from the center of the bubble to a distance of 0.1 times the radius. On this basis, the size of the light-emitting region would be of the order of perhaps 1% of the bubble radius or less. A direct test of this hypothesis does not appear straightforward. A consequence of the proposed mechanism would however be a lengthening of the duration of the light pulse as the sound intensity is lowered more and more toward threshold conditions, as in this case the radical production would be limited to the very center of the bubble.

## ACKNOWLEDGMENTS

The present study has been supported by NSF under grant CTS-8918144. F. N. E.'s participation has been supported by AFOSR grant AFOSR-85-0147.

Barber, B. P., Hiller, R., Arisaka, R., Fetterman, H., and Putterman, S. (**1992**). "Resolving the picosecond characteristics of synchronous sonoluminescence," J. Acoust. Soc. Am. **91**, 3061–3063.

Barber, B. P., and Putterman, S. (**1991**). "Observation of synchronous picosecond sonoluminescence," Nature **352**, 318–320.

Barber, B. P., and Putterman, S. (**1992**). "Light scattering measurements of the repetitive supersonic implosion of a sonoluminescent bubble," preprint.

Benjamin, T. B., and Ellis, A. T. (**1990**). "Self-propulsion of asymmetrically vibrating bubbles," J. Fluid Mech. **212**, 65–80.

Canuto, C., Hussaini, M. Y., Quarteroni, A., and Zang, T. A. (**1988**). *Spectral Methods in Fluid Dynamics* (Springer-Verlag, New York).

Cook, G. A. (**1961**). *Argon, Helium and the Rare Gases* (Interscience, New York), Vol. I.

Chambers, L. A. (**1936**). "The emission of visible light from pure liquids during acoustic excitation," Phys. Rev. **49**, 881.

Chambers, L. A. (**1937**). "The emission of visible light from cavitated liquids," J. Chem. Phys. **5**, 290–292.

Crum, L. A., and Reynolds, G. T. (**1985**). "Sonoluminescence produced by "stable" cavitation," J. Acoust. Soc. Am. **78**, 137–139.

Degrois, M., and Baldo, P. (**1974**). "A new electrical hypothesis explaining sonoluminescence, chemical actions and other effects produced in gaseous cavitation," Ultrasonics **12**, 25–28.

Egolfopoulos, F. N., and Law, C. K. (**1990**). "An experimental and computational study of the burning rates of ultra-lean to moderately-rich $H_2/O_2/N_2$ laminar flames with pressure variations," *Twenty-Third Symposium (International) on Combustion* (The Combustion Institute, City), pp. 333–340.

Eller, A. I., and Crum, L. A. (**1970**). "Instability of the motion of a pulsating bubble in a sound field," J. Acoust. Soc. Am. **47**, 762–767.

Flosdorf, E. W., Chambers L. A., and Malisoff, W. M. (**1936**). "Sonic activation in chemical systems: Oxidations at audible frequencies," J. Am. Chem. Soc. **58**, 1069–1076.

Flynn, H. G. (**1964**). "Physics of acoustic cavitation in liquids," in *Physical Acoustics*, edited by W. P. Mason (Academic, New York), Vol. I, Part B, pp. 57–172.

Frenkel', Ya. I. (**1949**). "Electrical effects associated with ultrasonically-induced cavitation in liquids," Zh. Fiz. Khim. **14**, 305–308.

Gaitan, D. F., and Crum, L. A. (**1990**). "Observation of sonoluminescence from a single cavitation bubble in a water/glycerine mixture," in *Frontiers of Nonlinear Acoustics, 12th ISNA*, edited by M. F. Hamilton and D. T. Blackstock (Elsevier, New York), pp. 459–463; "Sonoluminescence from single bubbles," J. Acoust. Soc. Am. Suppl. 1 **87**, S141.

Gaitan, D. F. (**1990**). "An experimental investigation of acoustic cavitation in gaseous liquids," Ph.D. thesis, University of Mississippi.

Gardiner, W. C., and Troe, J. (**1984**). *Combustion Chemistry*, edited by W. C. Gardiner (Springer-Verlag, New York), p. 173.

Gottlieb, D., and Orszag, S. A. (**1977**). *Numerical Analysis of Spectral Methods: Theory and Applications* (SIAM-CBMS, Philadelphia).

Greenspan, H. P., and Nadim, A. (**1993**). "On sonoluminescence of an oscillating bubble," Phys. Fluids A **5**, 1065–1067.

Griffing, V., and Sette, D. (**1955**). "Luminescence produced as a result of intense ultrasonic waves," J. Chem. Phys. **23**, 503–509.

Gunther, P., Heim, E., and Borgsted, H. O. (**1959**). "Uber die Kontinuerlichen Sonolumineszenzspektren Wassiriger Losungen," Z. Electrochem. **63**, 43–47.

Gunther, P., Heim, E., and Eichkorn, G. (**1959**). "Phasen-Korrelation Schallwechseldruck und Sonolumineszenz," Z. Angew. Phys. **11**, 274–277.

Harvey, E. N. (**1939**). "Sonoluminescence and sonic chemiluminescence," J. Am. Chem. Soc. **61**, 2392–2398.

Hickling, R. (**1963**). "Effects of thermal conduction in sonoluminescence," J. Acoust. Soc. Am. **35**, 967–974.

Horsburgh, S. (**1990**). "Radial instabilities of a pulsating air bubble in water," Ph.D. thesis, University of Mississippi.

Jarman, P. (**1960**). "Sonoluminescence: A Discussion," J. Acoust. Soc. Am. **32**, 1459–1462.

Kamath, V., and Prosperetti, A. (**1989**). "Numerical integration methods in gas bubble dynamics" J. Acoust. Soc. Am. **85**, 1538–1548.

Kee, R. J., Rupley, F. M., and Miller, J. A. (**1987**). "The CHEMKIN Thermodynamic Data Base," Sandia Report SAND87-8215.

Kuttruff, H. (**1962**). "Uber den zusammenhang zwischen der sonolumineszenz und der schwingungskavitation in flussigkeiten," Acustica **12**, 230–254.

Löfstedt, R., Barber, B. P., and Putterman, S. (**1993**). "Towards a hydrodynamic theory of sonoluminescence" (preprint).

Margulis, M. A. (**1969**). "Sonoluminescence and ultrasonic chemical reactions," Sov. Phys. Acoust. **15**, 135–151.

Negishi, K. (**1961**). "Experimental studies on sonoluminescence and ultrasonic cavitation," J. Phys. Soc. Jpn. **16**, 1450–1465.

Noltingk, B. E., and Neppiras, E. A. (**1950**). "Cavitation produced by ultrasonics," Proc. Phys. Soc. London **B63**, 674–685.

Nyborg, W. L., and Hughes, D. E. (**1967**). "Bubble annihilation in cavitation streamers," J. Acoust. Soc. Am. **42**, 891–894.

Parliz, U., Englisch, V., Scheffczyk, C., and Lauterborn, W. (**1990**). "Bifurcation structure of bubble oscillators," J. Acoust. Soc. Am. **88**, 1061–1077.

Plesset, M. S., and Prosperetti, A. (**1977**). "Bubble dynamics and cavitation," Ann. Rev. Fluid Mech. **9**, 145–185.

Prosperetti, A., Crum, L. A., and Commander, K. W. (**1988**). "Nonlinear bubble dynamics," J. Acoust. Soc. Am. **83**, 502–514.

Prosperetti, A. (**1984**). "Bubble phenomena in sound fields: part two," Ultrasonics **22**, 115–124.

Prosperetti, A. (**1991**). "The thermal behavior of oscillating gas bubbles," J. Fluid Mech. **222**, 587–616.

Prudhomme, R. O., and Guilmart, T. (**1957**). "Photogenese ultraviolette par irradiation ultrasonore de l'eau en presence des gaz rares," J. Chim. Phys. **54**, 336–340.

Roy, R. A., and Gaitan, D. F. (**1991**). "Experimental aspects of sonoluminescence," J. Acoust. Soc. Am. **89**, 1885 (A).

Saksena, T. K., and Nyborg, W. L. (**1970**). "Sonoluminescence from stable cavitation," J. Chem. Phys. **53**, 1722–1734.

Sehgal, C., Sutherland, R. G., and Verrall, R. E. (**1980**). "Optical spectra of sonoluminescence from transient and stable cavitation in water saturated with various gases," J. Phys. Chem. **84**, 388–395.

Sirotyuk, M. G. (**1966**). "Cavitation strength of water and its distribution of cavitation nuclei," Sov. Phys. Acoust. **11**, 318–322.

Suslick, K. S., Hammerton, D. A., and Cline Jr., R. E. (**1986**). "The sonochemical hotspot," J. Am. Chem. Soc. **108**, 5641–5642.

Suslick, K. S. (**1990**). "Sonochemistry," Science **247**, 1439–1445.

Taylor, K. J., and Jarman, P. D. (**1970**). "The spectra of sonoluminescence," Aust. J. Phys. **23**, 319–334.

Verrall, R. E., and Sehgal C. M. (**1988**). "Sonoluminescence," in *Ultrasound: its Chemical, Physical and Biological Effects*, edited by K. S. Suslick (VCH, New York), pp. 227–286.

Weyl, W. A., and Marboe, E. C. (**1949**). Research (London) **2**, 19–28.

Weyl, W. A. (**1951**). "Surface structure of water and some of its physical and chemical manifestations," J. Colloid Sci. **6**, 389–405.

Yetter, R. A., Dryer, F. L., and Rabitz, H. (**1991**). "A Comprehensive Reaction Mechanism for Carbon Monoxide/Hydrogen/Oxygen Kinetics," Combust. Sci. Technol. **79**, 97–120.